# Observations of Regional Seismic Discontinuities in the Earth's Upper Mantle from SS- and PP- precursors

**Lauren Waszek[1], Thuany Costa de Lima[2], Benoit Tauzin[3], Hrvoje Tkalčić[2], and Maxim Ballmer[4]**

[1]Physical Sciences, James Cook University, Australia
[2]Research School of Earth Sciences, The Australian National University, Australia
[3]Laboratoire de Géologie de Lyon, Lyon University, France
[4]Department of Earth Sciences, University College London, United Kingdom

Corresponding author: Thuany.CostadeLima@anu.edu.au

EGU General Assembly #EGU23 23 - 28 April 2023

Australian National University

Poster EGU23-16446

## Motivation

The distribution of seismic discontinuities between 250-350 km depth, also referred to as "X" discontinuity has been observed locally beneath subduction zones, both continental and oceanic crust, and some hotspots [1-7].

However, the detection of X-km is yet poorly resolved on a global scale, and causal mechanisms to justify its existence are debatable. A further discontinuity at 520 km depth is detected more frequently and is sometimes observed to be split into two signals[8-12].

Both discontinuities can be predicted by mineral phase transitions, however, parameters such as temperature and/or compositional heterogeneity associated with a basaltic fraction which contribute to their presence or absence, depth variation, strength, and/or splitting of signals are not fully understood, necessitating further investigations. Advancing the imaging of these discontinuities may provide insights into the thermal and chemical heterogeneities, and identify locations of hot materials, subducted oceanic crust remnants, or delaminated crustal roots.

## Data and method

We use precursors of SS and PP seismic phases recorded at receivers distributed globally.

SS and PP are shear and compressional seismic waves, respectively, that reflect at the Earth's surface, while their precursors are underside reflections at depths (**Figure 1**).

Our data were downloaded from IRIS using the epicenter distance range between 100°-180° for SS and 80°-140° for PP. Events considered are shallower than 75 km and 6.0 ≤ Mb ≤ 7.0, from July 1987 to December 2017.

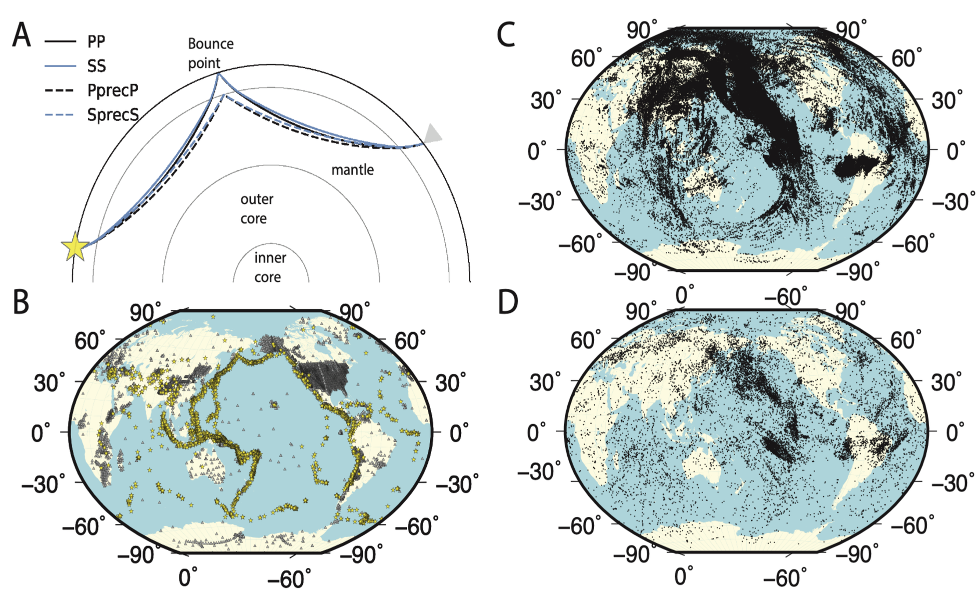


**Figure 1.** (A) Reflections of SS, PP, and their respective precursors' SdS, and PdP underneath a seismic discontinuity (for instance, the 300- or the 520-km). (B) Distribution of earthquakes (yellow stars) and receivers (grey triangles) used in this study. (C) Bounce points of the PP dataset (136512 records of 1668 earthquakes). (D) Bounce points of the SS dataset (58217 records of 2046 earthquakes).

This dataset has shown previous success in the global mapping of mid-mantle seismic discontinuities[13] and the mantle transition zone[14].

The seismograms are partitioned into spherical caps of 5°, 7.5°, 10°, and 15° radius and stacked into vespagrams, which are contour plots resulting from the summed traces of an array displayed as a function of slowness (**Figure 2**). Vespagrams are useful to reveal small but coherent signals that are not detected in seismograms.

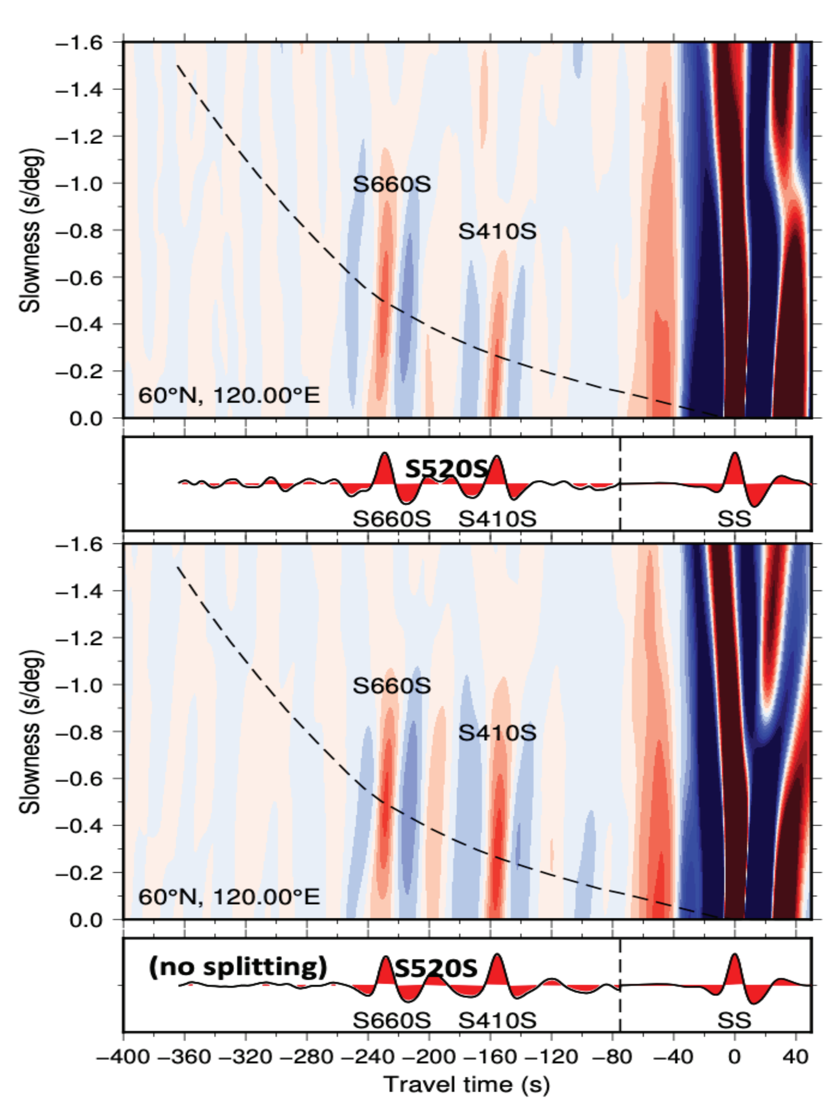


**Figure 2.** Slant-stack of SS seismograms showing identification of S520S precursor and comparison to synthetic calculated for a mechanical mixture of 20% basalt and 80% harzburgite. The waveforms at the bottom of each panel are the cross-sections indicated as dashed lines and normalized from 75s to 365s prior to the main phase to facilitate visual detection of the precursors.

## Thermochemical modelling

We use the reflectivity algorithm to generate synthetic seismograms for mechanical mixtures of basalt and harzburgite. We calculate a full catalogue of SS and PP synthetics which correspond to the real datasets, for our thermochemical model. This was generated by a Bayesian inversion of 410 and 660 depths and amplitudes, as measured from the same datasets14, 15 (Figure 3). This informs regarding locations where we may expect to observe features associated with the X and 520 discontinuities.

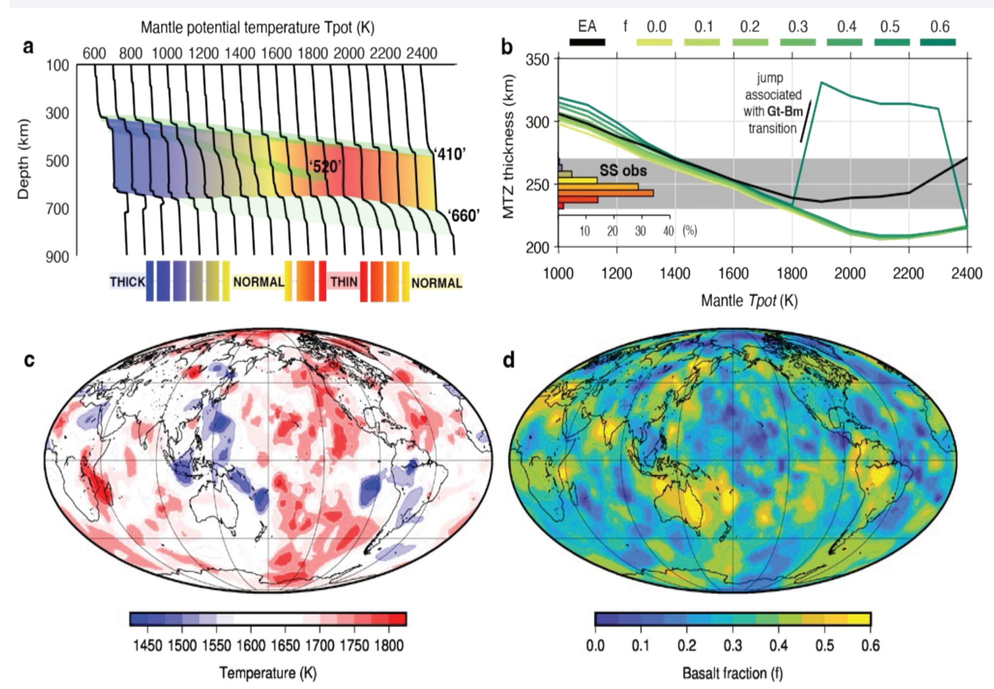


**Figure 3.** Thermochemical model of the MTZ from SS and PP precursors (adapted from Waszek et al., 2021 and Tauzin et al., 2022). a. Effects of temperature on MTZ thickness. b. Effects of composition on MTZ thickness. c, d. Thermal and chemical models generated from a Bayesian inversion of the 410 and 660 depths

Synthetics calculated for a full range of mantle models reveal that the visibilities of the X and 520 discontinuities in the SS and PP precursor data are highly dependent on thermochemistry (Figures 4, 5). Both signals appear visible in most models, but vary in depth and strength, and splitting in the case of 520. This variability suggests that a lack of visibility on global scales may be in part due to regional complexities. We also note that the signals are considerably more prominent in the SS data as compared to the PP data, and hence orient our primary observational analysis toward SS.

In summary, our synthetic modelling shows that the 520-km splits at lower temperatures, and the signal appears smaller at higher basaltic fractions. The "X" discontinuity is visible at higher temperatures and is larger in amplitude for higher basalt fractions.

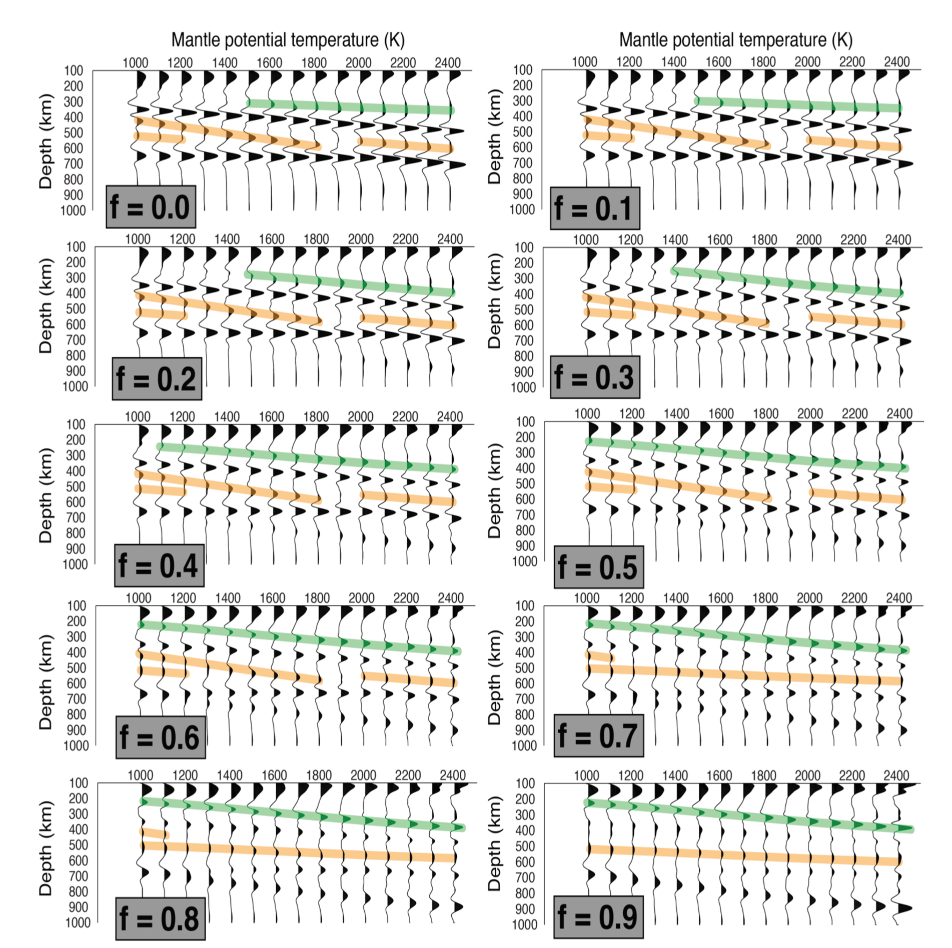


**Figure 4.** Synthetic SS waveforms as a function of T and composition of the basaltic fraction in percentage (figure adapted from Waszek et al., 2021). Green and orange dashed lines indicate our interpretation of the 300 km and 520 km, respectively.

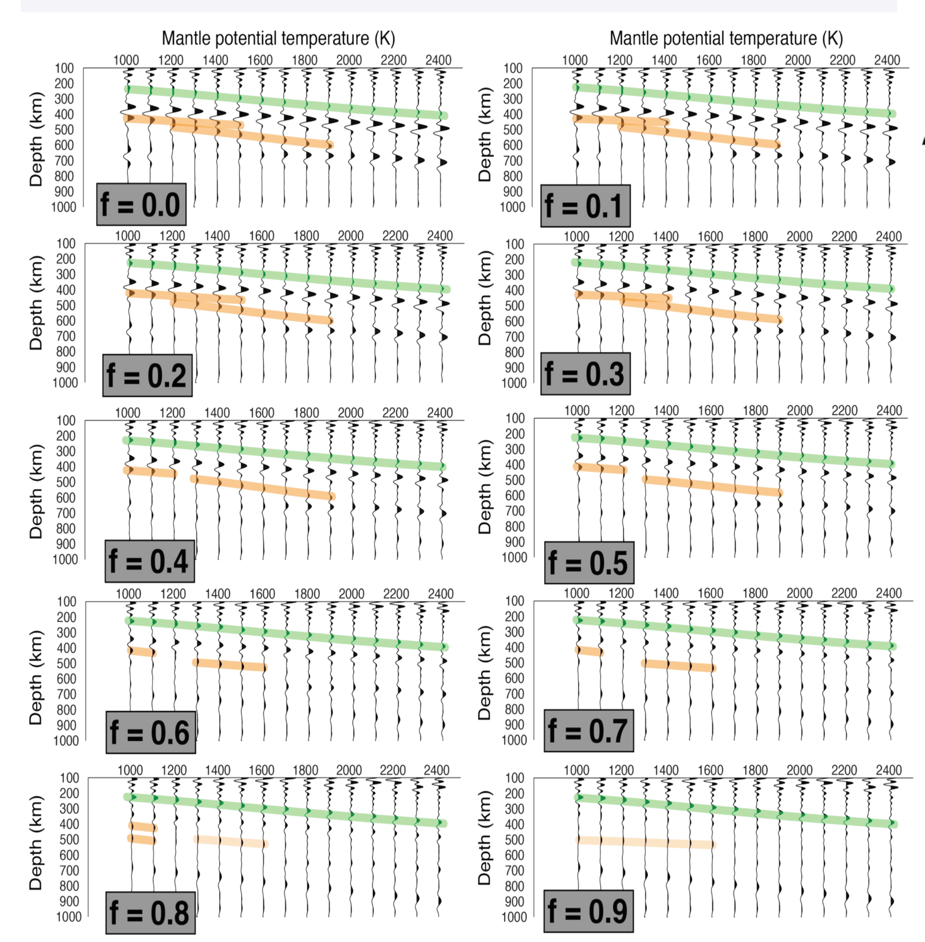


**Figure 5.** . Synthetic PP waveforms as a function of T and composition of the basaltic fraction in percentage (figure adapted from Waszek et al., 2021). Green and orange dashed lines indicate our interpretation of the 300 km and 520 km, re-

## Observations and on-going work

Signals arriving at times predicted with discontinuities at 300 km[2,7] and 520 km depth[11,12] are detected in our regional bins using for both SS and PP data. Consistent with these previous studies, we find a large quantity of detections on a global scale, with considerable variations in depth and amplitude. We are currently working on implementing a grid search method to model the waveforms considering variations in the depth of interfaces, seismic coverage, and noise level, simultaneously for the 410- and 300-km and 520- and 410 km.

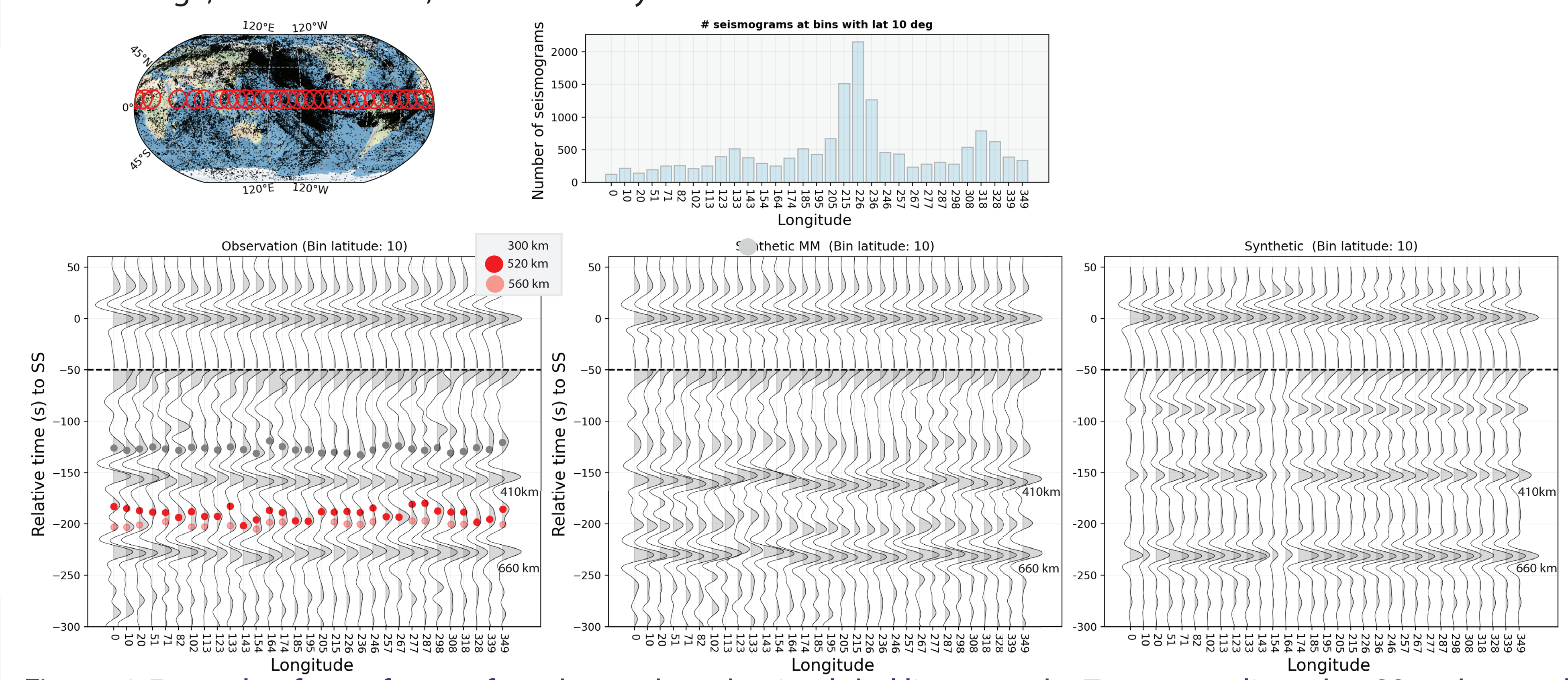


**Figure 6.** Example of waveforms of 520 km and 300 km in global linear stacks. Traces are aligned to SS and normalized to maximum amplitude in the window. Top-left figure, the SdS bounce points are in black dots. Red circles indicate the location of 10° radii near the equator. In the bottom-left figure, the travel-time picks of possible 300 km, 520 km, and 560 km. Bottom middle, the respective waveforms calculated using the thermochem. model with 20% harzburgite and 80% basaltic fraction[14], and the same source-station geometry as the observation. To the bottom right, the equivalent waveforms are calculated using the same source-station geometry as the observation, and PREM as the background model. To the top-right, the number of waveforms bouncing in each bin.

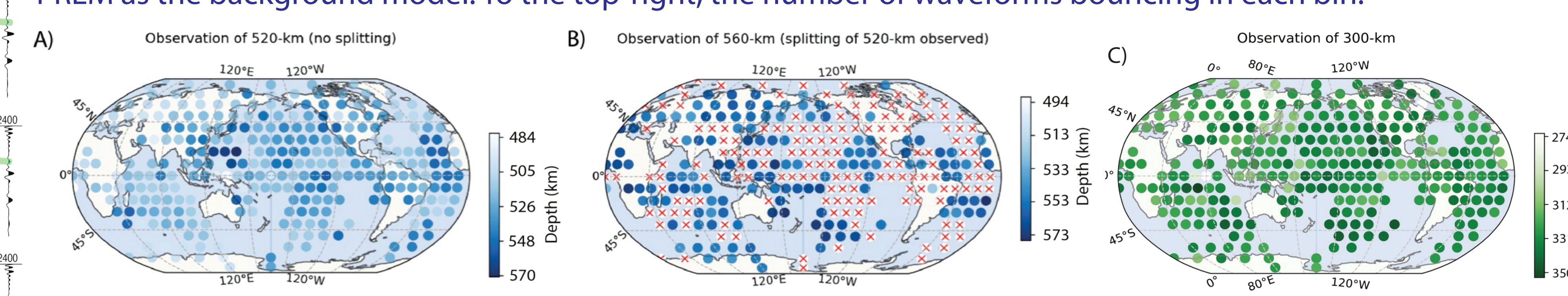


**Figure 7.** Observations of 520 splitting in SS data. (A) Observability of 520 km signals (B) Detection and observability of 560 km signals. White circles indicate lack of split signals of 520 km. (C) Detection of 300km.

## Conclusions

- We perform a systematic search for global-scale discontinuities at 300- and 500-km depths, in order to investigate their seismic signatures, determine probable temperatures and compositions, and with the goal of interpreting our results in the context of global geodynamical circulation patterns.
- Our method utilizes large global seismic datasets of SS and PP precursors, coupled with mineral physics modelling for a range of realistic mantle temperatures and composition. We analyse our results in the context of our recent thermochemical model for the mantle transition zone.
- Our results indicate the presence of both 300- and 520-km discontinuities in the global observations, as predicted by mineral physics modelling. Since the discontinuity characteristics are primarily dependent on basalt fraction rather than temperature, our work will inform regarding the presence of compositional layering, and the evolution of mantle convection on regional and global scales.

1. Revenaugh, J., and T. H. Jordan (1991), Mantle layering from ScS reverberations: 3. the upper mantle, J. Geophys. Res. Solid Earth, 96(B12), 19,781–19,810, doi: 10.1029/91jb01487.
2. Schmerr, N. C., Kelly, B. M., & Thorne, M. S. (2013). Broadband array observations of the 300 km seismic discontinuity. Geophysical Research Letters, 40(5). https://doi.org/10.1002/grl.50257
3. Schmerr, N. (2015), Imaging mantle heterogeneity with upper mantle seismic discontinuities, in The Earth's Heterogeneous Mantle, pp. 79–104, Springer International Publishing, doi:10.1007/978-3-319-15627-9 3.
4. Deuss, A., and J. H. Woodhouse (2002), A systematic search for mantle discontinuities using SS-precursors, Geophys. Res. Lett., 29 (8), 90–1.
5. Deuss, A., and J. H. Woodhouse (2004), The nature of the Lehmann discontinuity from its seismological Clapeyron slopes, Earth Planet. Sci. Lett., 225(3-4), 295– 304, doi:10.1016/j.epsl.2004.06.021.
6. Kemp, M., J. Jenkins, J. Maclennan, and S. Cottaar (2019), X-discontinuity and transition zone structure beneath Hawaii suggests a heterogeneous plume, Earth Planet. Sci. Lett., 527, 115,781, doi:10.1016/j.epsl.2019.115781.
7. Pugh, S., Jenkins, J., Boyce, A., & Cottaar, S. (2021). Global receiver function observations of the X-discontinuity reveal recycled basalt beneath hotspots. Earth and Planetary Science Letters, 561. https://doi.org/10.1016/j.epsl.2021.116813
8. Shearer, P.M., 1990. Seismic imaging of upper-mantle structure with new evi- dence for a 520-km discontinuity. Nature 344, 121–126. https://doi.org/10.1038/ 344121a0.
9. Shearer, P.M., 1991. Constraints on upper mantle discontinuities from observa- tions of long-period reflected and converted phases. J. Geophys. Res. 96 (B11), 18147–18182. https://doi.org/10.1029/91jb01592.
10. Cummins, P.R., Kennett, B.L.N., Bowman, J.R., Bostock, M.G. (1992). The 520-km discontinuity. Bull. Seismol. Soc. Am. 82 (1), 323–336.
11. Deuss, A., and J. Woodhouse (2001), Seismic observations of splitting of the mid-transition zone discontinuity in Earth's mantle, Science, 294 (5541), 354–357, doi: 10.1126/science.1063524.
12. Tian, D., Lv, M., Wei, S. S., Dorfman, S. M., & Shearer, P. M. (2020). Global variations of Earth's 520- and 560-km discontinuities. Earth and Planetary Science Letters, 552. https://doi.org/10.1016/j.epsl.2020.116600
13. Waszek, L., Schmerr, N. C., & Ballmer, M. D. (2018). Global observations of reflectors in the mid-mantle with implications for mantle structure and dynamics. Nature Communications, 9(1).
14. Waszek, L., Tauzin, B., Schmerr, N. C., Ballmer, M. D., & Afonso, J. C. (2021). A poorly mixed mantle transition zone and its thermal state inferred from seismic waves. Nature Geoscience.